Detailed Model of the Aggregation Event between Two Fractal Clusters

Marco Lattuada, Hua Wu, Jan Sefcik, and Massimo Morbidelli*

Institute for Chemical and Bioengineering, Department of Chemistry and Applied Biosciences, ETH Zurich, Hönggerberg HCI, 8093 Zurich, Switzerland

Received: November 11, 2005; In Final Form: February 22, 2006

A model has been developed for describing the aggregation process of two fractal clusters under quiescent conditions. The model uses the approach originally proposed by Smoluchowski for the diffusion-limited aggregation of two spherical particles but accounts for the possibility of interpenetration between the fractal clusters. It is assumed that when a cluster diffuses toward a reference cluster their center-to-center distance can be smaller than the sum of their radii, and their aggregation process is modeled using a diffusion-reaction equation. The reactivity of the clusters is assumed to depend on the reactivity and number of their particles involved in the aggregation event. The model can be applied to evaluate the aggregation rate constant as a function of the prevailing operating conditions by simply changing the value of the particle stability ratio, without any a priori specification of a diffusion-limited cluster aggregation, reaction-limited cluster aggregation, or transition regime. Furthermore, the model allows one to estimate the structure properties of the formed cluster after the aggregation, based on the computed distance between the aggregating clusters in the final cluster.

1. Introduction

Aggregation of colloidal dispersions has been a research topic of great relevance in colloidal science,[1,2] also because various industrial applications involving colloidal dispersions require a controlled aggregation step to obtain the desired final products. Thus, in the last 20 years a large number of experimental and theoretical studies have been carried out aiming at understanding the physical principles of the aggregation phenomena.[3−10]

Several experimental techniques, such as light, neutron, and X-ray scattering and electron and confocal microscopy, have been applied to investigate colloidal aggregations. These studies have clarified that there exist two well-defined aggregation regimes under stagnant conditions: the fast or diffusion-limited cluster aggregation (DLCA) regime and the slow or reaction-limited cluster aggregation (RLCA) regime.[5] The two regimes are characterized by different structures of the formed clusters, which are more compact in the RLCA regime than in the DLCA regime.[3,4] From the modeling perspective, several approaches such as Monte Carlo simulations, Brownian dynamic simulations, and the kinetic approach based on the population balance equations have been applied to describe these aggregation processes. The main objective of using Monte Carlo simulations[11−14] is to reproduce the fractal structures of the formed clusters rather than to model the time evolution of the cluster mass distribution. Although Brownian dynamic simulation[15,16] allows one to investigate the real-time evolution of both structure and mass of the clusters, it requires an enormous computational time, so that only small size systems can be dealt with. The kinetic approach based on the population balance equations (PBEs)[17−20] is probably the most suitable approach for the purpose of process design, since it allows one to investigate the time evolution of the cluster mass distribution without limitations in the size of the aggregating system, although it does not provide any information about the cluster structure.

* Author to whom correspondence should be addressed. Phone: 0041-44-6323034. E-mail: morbidelli@chem.ethz.ch.

The kinetic approach assumes that the aggregation event between two clusters is a second-order process, so that the time evolution of the cluster mass distribution is described by the following PBEs in discrete form[19]

$$\frac{dN_i(t)}{dt} = -\sum_{j=1}^{\infty} K_{i,j} Ni(t) Nj(t) + \frac{1}{2}\sum_{j=1}^{i-1} K_{i-j,j} N_{i-j}(t) N_j(t) \quad (1)$$

where $K_{i,j}$ is the aggregation rate constant (referred to as the aggregation kernel) between two clusters with masses i and j and $N_i(t)$ is the number concentration of the clusters with mass i. The major difficulty in using these PBEs is that one needs to identify a proper aggregation kernel, which requires a priori structural information about clusters as well as knowledge of the aggregation mechanism.

Finding a suitable expression for the aggregation kernel is, in general, a difficult task, because the strong interplay between aggregation mechanism and cluster structure makes the problem hard to tackle, particularly in the case of shear-induced aggregation, where the structure of clusters may change progressively with time. For this reason, most of the work has been done under stagnant DLCA or RLCA conditions, because it is well-known that DLCA or RLCA clusters follow fractal scaling, and the self-similarity nature of fractal objects implies that the structure does not change during the aggregation. However, even for stagnant aggregation processes, the available expressions for the aggregation kernel in the literature are usually semiempirical. They were derived on the basis of physical principles only for the aggregation process between spherical primary particles[21,22] and then extended empirically to fractal clusters. As an example, the following expression for the DLCA kernel $K_{i,j}$ has been proposed[13,19]

$$K_{i,j} = \frac{8k_B T}{3\eta W} \frac{(i^{1/D_f} + j^{1/D_f})(i^{-1/D_f} + j^{-1/D_f})}{4} \quad (2)$$

where W is the Fuchs stability ratio accounting for hydrody-

10.1021/jp056538e CCC: $33.50
Published on Web 03/16/2006

namic and van der Waals interactions between particles and usually has a value around 2, T is the absolute temperature, η is the fluid dynamic viscosity, k_B is the Boltzmann constant, and D_f is the cluster fractal dimension, equal to about 1.8 in the case of DLCA clusters. The term $8k_BT/3\eta W$ on the right-hand side of eq 2 represents the aggregation kernel of primary particles in diluted conditions, while the second term accounts for changes in collision area and diffusion coefficients of the two fractal clusters. Despite this empiricism, the predictions of eq 1 with eq 2 are in good agreement with experimental data obtained from the growth of clusters under DLCA conditions.

For the aggregation kernel under RLCA conditions, the situation is even more uncertain. Probably the most widely accepted RLCA kernel is the so-called product kernel

$$K_{i,j} = \frac{8k_BT}{3\eta W}\frac{(i^{1/D_f} + j^{1/D_f})(i^{-1/D_f} + j^{-1/D_f})}{4}(ij)^{\lambda} \qquad (3)$$

It has been found[20] that this kernel can reproduce experimental data under dilute RLCA conditions for fluorinated polymer latexes with a value of $\lambda = 0.4$. A slightly smaller λ value has been obtained by Odriozola et al.[24] by fitting Monte Carlo data. Equation 3 indicates that the RLCA kernel is equal to the DLCA kernel multiplied by an empirical term containing the product of the masses of the two clusters. This simple functional form arises from the observation that the reactivity is larger for larger fractal clusters, and the product term $(ij)^{\lambda}$ in eq 3 accounts for this increase in reactivity. A partial justification of the product term has been given by Axford,[9] who, on the basis of geometry of fractal clusters, derived a value of $\lambda = 0.5$. However, the larger reactivity of larger clusters is also supported by Monte Carlo simulations and experiments,[3,4] which indicate that wider cluster mass distributions are obtained under RLCA than under DLCA conditions.

One of the major drawbacks of eq 3 is that it leads to unrealistic results when the value of the product term becomes larger than that of the stability ratio W. This would mean that the aggregation rate constant for substantially large clusters could be larger than that under diffusion-limited conditions. This is of course not acceptable, since the aggregation process is always limited by diffusion. This situation is referred to as crossover to DLCA.[3,23] Recently, Odriozola et al.[24] have proposed a new kernel based on a probabilistic model, which correctly predicts the crossover to DLCA, and has the following form

$$K_{i,j} = \frac{8k_BT}{3\eta W}\frac{(i^{1/D_f} + j^{1/D_f})(i^{-1/D_f} + j^{-1/D_f})}{4}\frac{N_{1,1}(ij)^{\lambda}}{1 + \frac{[N_{1,1}(ij)^{\lambda} - 1]}{W}} \qquad (4)$$

where $N_{1,1}$ is defined as the mean number of collisions per event between a pair of particles. In a recent work[20] we have demonstrated that during the initial stages of aggregation the two kernels, eqs 3 and 4 with $N_{1,1} = 1$, lead to the same results. Still, the physical meaning of the exponent λ is not clear even from eq 4.

Besides those mentioned above, several other semiempirical aggregation kernels may be found in the literature.[19] However, there are, to our knowledge, very few studies in the literature that attempt to derive in a more rigorous way the aggregation rate between fractal clusters.[25,26] It is worth mentioning the work by Zurita-Gotor and Rosner,[25] who have calculated the rate of collision of fractal clusters in the so-called free molecular regime, i.e., in the situation where the solvent is a gas of so low density that the mean free path of gas molecules is larger than the average size of the particles. In this case, the trajectories of particles and clusters are straight lines. Such a situation is typical for soot clusters formed in flames. The advantage of dealing with the aggregation of clusters in the free molecular regime is that some results from the kinetic theory of gases can be applied to estimate the average aggregation rate. However, neither the results nor the method presented by Zurita-Gotor and Rosner[25] can be easily extended to the DLCA and RLCA processes in liquid colloidal dispersions.

In this work, we attempt to give a more physically sound background to the DLCA and RLCA kernels discussed above. In particular, we propose a model for the aggregation event of two fractal clusters, valid in both DLCA and RLCA conditions, which allows one to compute the above-mentioned kernels. The proposed approach is a generalization of Smoluchowski theory, originally proposed for the aggregation of spherical primary particles, by accounting for the fractal nature of clusters. In particular, we solve the diffusion equation for the clusters that diffuse toward a reference cluster and consider that fractal clusters can interpenetrate due to their open structure. To validate the newly developed model we compare its predictions with those of eqs 2 and 4, which, having received quite a bit of support by comparisons with experimental data, may be regarded at the moment as the reference, although empirical, models. Moreover, it will be seen that on the basis of the present model one may obtain information about the structure of the cluster formed as a result of the aggregation event.

2. The Aggregation Model

2.1. Main Assumptions. *2.1.1. Generalization of the Smoluchowski Approach.* The approach used in this work in modeling the aggregation event of two clusters is a generalization of Smoluchowski method.[21] Smoluchowski modeled the aggregation rate of colloidal particles by calculating the rate of diffusion of particles toward a central reference particle. In particular, the rate of diffusion of particles toward the reference one is obtained by solving the steady-state diffusion equation in spherical coordinates to obtain the total diffusive flux of particles toward the reference particle, with the assumption that the concentration of particles approaches zero at the collision surface of the reference particle. Furthermore, in computing the total aggregation rate of a given number of particles, all of the particles in the system are considered as reference particles. This is clearly a mean-field approach, valid for low particle volume fractions, where multibody interactions are negligible. The model that we propose relies also on the mean-field approach. The main difference between the Smoluchowski and the present approach is that we do not deal with impenetrable solid spherical particles but rather with fractal clusters, which due to their open structure can interpenetrate during the aggregation. In other words, it is assumed that the aggregation between the fractal clusters *does not necessarily occur* at the point where their outer shells touch.

2.1.2. Reactivity of Particles in Clusters. Another important difference between the Smoluchowski and the present model is the way of dealing with the RLCA processes. Fuchs extended the Smoluchowski theory to account for aggregation of primary particles in the presence of interparticle interactions. This leads to the introduction of an efficiency coefficient in the expression of the aggregation rate, which is the inverse of the Fuchs stability ratio W. In principle, the W value can be computed using the

following expression when the details of the interparticle interactions are known

$$W = 2\int_2^\infty \frac{e^{U/k_BT}}{G(l)l^2}\,dl \tag{5}$$

where U is the sum of van der Waals attractive and electrostatic repulsive interaction energies between two particles, l is the dimensionless center-to-center distance normalized to the particle radius, and G accounts for the additional resistance caused by the squeezing of the fluid during the particle approach. Thus, the reaction-limited aggregation between two particles corresponds to the situation where some electrostatic repulsion among the particles exists, which significantly slows down the aggregation rate. The detailed treatment of the electrostatic repulsion between two spherical particles in a solution containing electrolytes requires in general the solution of the Poisson−Boltzmann equation[1] for the electrostatic potential, from which the electrostatic free energy of interaction can be evaluated, leading to the estimate of W using eq 5. It should be pointed out that for fractal clusters aggregating in the reaction-limited regime a detailed modeling of their interactions is difficult. This would require the solution of the Poisson−Boltzmann equation for a system with a very irregular geometrical structure. In addition, the computation should be carried out independently for many different pairs of clusters at given masses with detailed configurations, and then the results should have to be averaged over all the pairs. Clearly, to overcome all of these difficulties some additional drastic assumptions are needed.

In this work, we assume that the reactivity of the particles belonging to the cluster is equal to the reactivity of isolated particles under the same conditions as in the cluster. This means that the electrostatic energy of a particle is not significantly perturbed by the presence of the other neighbor particles in the cluster. This assumption is based on the fact that under typical RLCA conditions (even for W values on the order of $\sim 10^7$) the electrostatic interaction energy of two approaching particles becomes significant only when their distance is on the order of a few nanometers, while the typical particle diameter is several tens of nanometers. Consequently, it is reasonable to assume that as two clusters approach the interactions experienced by two particles belonging to the clusters are very similar to the interactions experienced by two isolated particles located at the same distance. As a result, we consider in our model that the very particles of the cluster are responsible for the aggregation. In other words, the reactivity of a cluster depends on the number of its particles that are involved in the aggregation event. It is evident that in this way the larger is the cluster, the more the possibility for it to aggregate, because of the larger number of particles that can connect to the other approaching cluster.

2.1.3. Clusters as Spherically Symmetric Objects. The fractal clusters used for modeling the aggregation events are taken from Monte Carlo simulations. In particular, for a cluster with mass i, its radial particle density, $\rho_i(r)$, is obtained by averaging the radial particle density of at least 1600 clusters of the same mass, and the average cluster is then assumed to be spherically symmetric. Details of this averaging process are reported elsewhere.[27] It was found that the radial particle density $\rho_i(r)$ can be expressed as[27]

$$\rho_i(r) = Ar^\beta \exp\left[-\left(\frac{r}{R_c}\right)^z\right] \tag{6}$$

where A, β, and z are empirical parameters and R_c is the cutoff length. Expressions for all these parameters are listed in Table 1 as a function of the mass i, where D_f is the fractal dimension, whose value is 1.85 and 2.05 for DLCA and RLCA clusters, respectively. It should be noted that the $\rho_i(r)$ value given by eq 6 approaches zero only when $r \to \infty$. Therefore, it is necessary to define a maximum size of the cluster with mass i, referred to as $R_{s,i}$, beyond which the particle density can be considered to be zero. In this work, such a $R_{s,i}$ value is defined as the r value that includes 99.9% of the total cluster mass, i.e.,

TABLE 1: Expressions for the Parameters Involved in Computing the Radial Density Distribution, $\rho_i(r)$ Given by Eq 6, under Both DLCA and RLCA Conditions[27]

$A = (iz/4\pi\Gamma(3+\beta/z)R_c^{3+\beta})$
Γ is the Euler gamma function[28]

$\beta = z(r^*/R_c)^z$

$z = d((i-e)^m/(i-e)^m+f)$
DLCA: $d = 1.6273$, $e = -0.1656$, $f = -0.5034$, $m = 1$
RLCA: $d = 1.488$, $e = -0.1779$, $f = -0.6492$, $m = 1$

$R_c = pR_p i^{1/D_f}$
$p = 0.6$ for both DLCA and RLCA

$r^* = R_p a i^b$;
DLCA: $a = 0.454$, $b = 0.361$
RLCA: $a = 0.464$, $b = 0.353$

$$0.999i = 4\pi \int_0^{R_{s,i}} \rho_i(r) r^2\,dr \tag{7}$$

It is found that the above condition is always satisfied if we set $R_{s,i} = 3.3R_c$. An example is given in Figure 1, where the radial particle density profiles of a DLCA and a RLCA cluster (both containing 100 primary particles) are shown. It can be seen that the density in the inner part is larger for the RLCA cluster than for the DLCA cluster, but for the RLCA cluster, as expected, the decay of $\rho_i(r)$ with r is faster, leading to a smaller $R_{s,i}$ value with respect to that of the DLCA cluster of the same mass.

It is worth noting that the above assumption that clusters are spherically symmetric objects leads to significant simplification of the mathematical formulation of the model reported in the following. This would be intractable if one considered aggregation between two fractal clusters of arbitrary geometry.

2.2. Mathematical Formulation. *2.2.1. The Basic Equation.* On the basis of the Smoluchowski mean-field approach,[21] let us consider a cluster as the reference and investigate the relative diffusive motion of the other clusters toward the reference. In the following, we always take the cluster with the largest mass

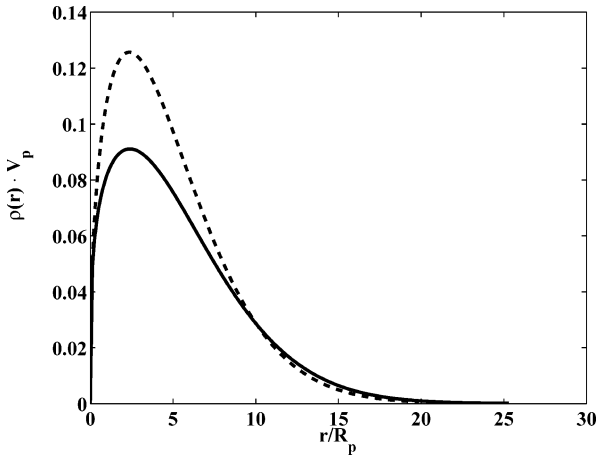

Figure 1. Radial particle density, $\rho(r)$, computed through eq 6, multiplied by the particle volume, $V_p = (4/3)\pi R_p^3$, as a function of the dimensionless radial distance for a DLCA cluster (solid curve) and a RLCA cluster (broken curve), both containing 100 particles.

as the reference, and its properties are labeled using the subscript i, while the properties of the other clusters are labeled using the subscript j, and obviously, $i \geq j$.

To describe the diffusive motion of a cluster toward the reference one, one needs to distinguish two situations, i.e., whether the two clusters are interpenetrated. We refer to the region where no interpenetration occurs (i.e., the distance r between the centers of the two clusters is larger than the sum of their radii, $r \geq R_{s,i} + R_{s,j}$) as the outer region, and the region where interpenetration occurs (i.e., $r < R_{s,i} + R_{s,j}$) as the inner region.

In the outer region, the diffusive motion of the clusters can be described using the usual steady-state diffusion equation, and the radial number concentration profile $N_j(r)$ of the diffusing clusters is a solution of the Laplace equation written in spherical coordinates

$$\frac{1}{r^2}\frac{d}{dr}\left[D_{i,j}{}^0 r^2 \frac{dN_j(r)}{dr}\right] = 0 \tag{8}$$

where $D_{i,j}{}^0$ is the mutual diffusion coefficient of two clusters with masses i and j, computed using the Stokes−Einstein formula

$$D_{i,j}{}^0 = \frac{k_B T}{6\pi\eta}\left(\frac{1}{R_{h,i}} + \frac{1}{R_{h,j}}\right) \tag{9}$$

where $R_{h,i}$ and $R_{h,j}$ are the hydrodynamic radii of the two clusters.

In the inner region where interpenetration among the clusters occurs, the reaction, i.e., the aggregation between the clusters, has to be accounted for. This is done by introducing in eq 8 a reaction term, and the problem is reduced to the solution of the following diffusion-reaction equation to obtain the radial number concentration profile of the diffusing clusters

$$\frac{1}{r^2}\frac{d}{dr}\left[D_{i,j}(r) r^2 \frac{dN_j(r)}{dr}\right] = k^*_{i,j}(r) N_j(r) \tag{10}$$

where $D_{i,j}(r)$ is the radial-dependent mutual diffusion coefficient and $k^*_{i,j}(r)$ is the local reaction rate between clusters i and j, with $r < R_{s,i} + R_{s,j}$. Note that the hydrodynamic and colloidal interactions have been considered in the expression for the local reaction rate while their effect on the cluster trajectory is ignored because the typical length scale of such interactions is substantially smaller than the size of a cluster. The radial dependency of the local reaction rate arises because of the model assumption discussed above that the reactivity of a cluster depends on the number of its particles that can participate in the reaction. Two parameters can affect the number of the particles participating in the reaction, the overlapping volume between the two clusters V and the radial particle density profile in the clusters $\rho_i(r)$. The former increases as the centers of the two clusters come closer, because the clusters have been assumed to be spherically symmetric objects. The latter is given by eq 6 and increases as the distance r moves from the external surface toward the center of the cluster, as clearly shown in Figure 1. Thus, the number of particles participating in the reaction increases substantially as the center-to-center distance between two clusters decreases. Similarly, the mutual diffusion coefficient of the two clusters also depends on the extent of the interpenetration in the inner region, because the increase in the number of particles in the overlapping volume can hinder the mutual diffusion of the clusters.

Thus, in summary, the basic equation discussed above is composed of two second-order linear differential equations (eqs 8 and 10), corresponding to the outer and inner regions, respectively

$$\begin{cases} \dfrac{1}{r^2}\dfrac{d}{dr}\left[D_{i,j}{}^0 r^2 \dfrac{dN_j(r)}{dr}\right] = 0 & \text{if } r > R_{s,i} + R_{s,j} \\ \dfrac{1}{r^2}\dfrac{d}{dr}\left[D_{i,j}(r) r^2 \dfrac{dN_j(r)}{dr}\right] = k^*_{i,j}(r) N_j(r) & \text{if } r < R_{s,i} + R_{s,j} \end{cases} \tag{11}$$

where $D_{i,j}(r)$ and $k^*_{i,j}(r)$ need to be defined.

2.2.2. The Case of Particle−Cluster Aggregation−Estimation of $D_{i,1}(r)$ and $k^*_{i,1}(r)$. Let us first consider the simple case where the smallest cluster is a primary particle. Then, the problem reduces to the aggregation between a particle and a fractal cluster. In this case, the hindrance encountered by a particle diffusing into a cluster is proportional to the local solid volume fraction within the cluster, which is equal to the radial particle density times the particle volume. This is equivalent to assuming that the diffusion coefficient of a particle inside a cluster is proportional to the local cluster porosity. Therefore, the radial dependence of the mutual diffusion coefficient between a particle and a cluster can be modeled as

$$D_{i,1}(r) = D_{i,1}{}^0\left[1 - \frac{4}{3}\pi R_p{}^3 \rho_i(r)\right] \tag{12}$$

where the mutual diffusion coefficient in the outer region, $D_{i,1}{}^0$, is given by eq 9.

Consistently, the local reaction rate of a diffusing particle with a cluster is given by the local particle density within the cluster, $\rho_i(r)$, times the collision rate between the diffusing particle and the particles belonging to the cluster. It is assumed that the latter is given by the collision rate of particles derived by Smoluchowski,[21] but in the present case, the mobility of the particles belonging to the cluster is naturally equal to that of the cluster, i.e., based on $1/R_{h,i}$ instead of $1/R_p$. Thus, it follows that

$$k^*_{i,1}(r) = \alpha\rho_i(r)\frac{4k_B T}{3\eta W} R_p\left(\frac{1}{R_p} + \frac{1}{R_{h,i}}\right) \tag{13}$$

where W is the Fuchs stability ratio, which, as discussed above, is estimated based on the interactions between two isolated particles. The parameter α in eq 13 is the effectiveness factor of collision area. Its introduction is based on the fact that a particle belonging to a cluster connects at least to another particle, leading to at least 30% of its area being unaccessible for the collision. Since the average number of nearest neighboring particles in a cluster is approximately 2,[29] the α value should be in the range of 0.25−0.5.

2.2.3. The Case of Cluster−Cluster Aggregation−Estimation of $D_{i,j}(r)$ and $k^*_{i,j}(r)$. In the case of two clusters, the situation is more complicated. When interpenetration between two clusters occurs, all of the particles in the overlapping volume can contribute to the hindrance experienced by the clusters during their mutual diffusion and to the reaction rate. Thus, in estimating the mutual diffusion coefficient, $D_{i,j}(r)$, one has to account for the hindrance arising from the entire overlapping volume between the two clusters, V. Similarly, in the computation of the aggregation rate, $k^*_{i,j}(r)$, one has to account for the aggregation occurring between any pair of particles in the two clusters in the overlapping volume V. For computing $D_{i,j}(r)$, we assume that the hindrance resulting from all the particles is

additive. Then, since the number of particles belonging to the cluster with mass j in a volume dV is equal to ρ_jdV and the fraction of space occupied by particles belonging to the cluster with mass i is given by $(4/3)\pi R_p^3 \rho_i$, it follows that

$$D_{i,j}(r) = D_{i,j}^0\left(1 - \frac{4}{3}\pi R_p^3 \int_V \rho_i \rho_j \, dV\right) \quad (14)$$

For the calculations of $k_{i,j}^*(r)$, the contributions to the reaction from all of the particles in V have to be summed

$$k_{i,j}^*(r) = \alpha \frac{4k_B T}{3\eta W} R_p \left(\frac{1}{R_{h,j}} + \frac{1}{R_{h,i}}\right)\left(\int_V \rho_i \rho_j \, dV\right) \quad (15)$$

Note that the mobility of the particles is equal to the mobility of the cluster to which they belong.

At this point, it is necessary to evaluate the integral that appears in both eqs 14 and 15. Recall that the fractal clusters have been assumed to be spherically symmetric objects. Then, the overlapping region of the two clusters is represented by two symmetric spherical caps. The integral can be performed by using spherical coordinates centered at the center of cluster i, taking advantage of the rotational symmetry of the system with respect to the line going through the centers of the two clusters. In this manner, when eq 6 is used for the radial particle densities, the integral can be written in the following form

$$\int_V \rho_i \rho_j \, dV = 2\pi A_i A_j \int_{low}^{up} x^{\beta_i+2} \exp\left[-\left(\frac{x}{R_{c,i}}\right)^{z_i}\right] dx \int_0^{\theta^*} y^{\beta_j} \times \exp\left[-\left(\frac{y}{R_{c,j}}\right)^{z_j}\right] \sin(\theta^*) \, d\theta \quad (16)$$

where y and θ^* are given by

$$y^2 = x^2 + r^2 - 2xr\cos(\theta) \quad (17)$$

and

$$\theta^* = \begin{cases} \arccos\left(\dfrac{r^2 + x^2 - R_{s,j}^2}{2rx}\right) & \text{if } r + x > R_{s,j} \\ \pi & \text{if } r + x < R_{s,j} \end{cases} \quad (18)$$

It is clear that the integral with respect to the angular variable θ can be performed analytically. Thus, after proper analytical manipulations, we obtain

$$\int_V \rho_i \rho_j \, dV = \frac{2\pi A_i A_j R_{c,j}^{\beta_j+2}}{r z_j} \Gamma\left(\frac{\beta_j + 2}{z_j}\right) \int_{low}^{up} x^{\beta_i+1} \times \exp\left[-\left(\frac{x}{R_{c,i}}\right)^{z_i}\right] \left(\Gamma_{inc}\left[\left(\frac{sup}{R_{c,j}}\right)^{z_j}, \frac{2+\beta_j}{z_j}\right] - \Gamma_{inc}\left[\left|\frac{r-x}{R_{c,j}}\right|^{x_j}, \frac{2+\beta_j}{z_j}\right]\right) dx \quad (19)$$

where Γ and Γ_{inc} are the Euler gamma and incomplete gamma functions, respectively.[28] The integration interval parameters, low, up, and sup, are given by

$$low = \begin{cases} 0 & \text{if } r < R_{s,j} \\ r - R_{s,j} & \text{if } r > R_{s,j} \end{cases} \quad (20)$$

$$up = \min\{r + R_{s,j}, R_{s,i}\} \quad (21)$$

$$sup = \begin{cases} r + x & \text{if } r + x < R_{s,j} \\ R_{s,j} & \text{if } r + x > R_{s,j} \end{cases} \quad (22)$$

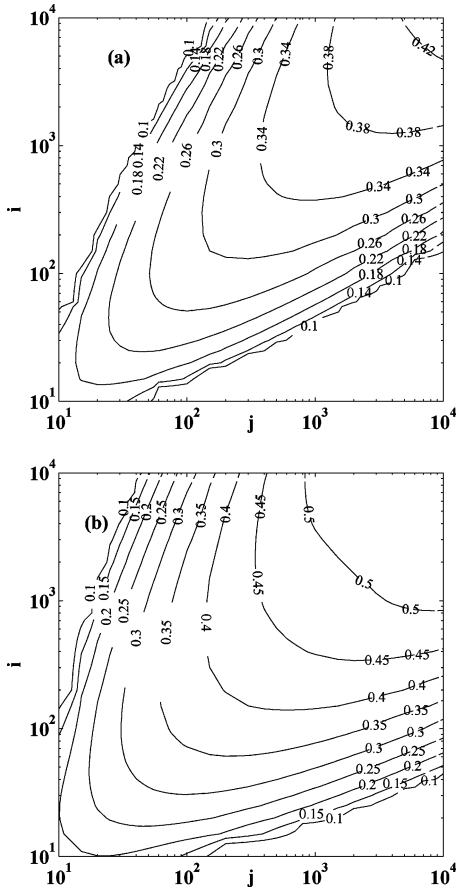

Figure 2. Values of the normalized minimum approaching distance between clusters with masses i and j, $r'/(R_{s,i} + R_{s,j})$, as a function of i and j, in the form of level curves: (a) DLCA clusters; (b) RLCA clusters.

The initial volume integral has been reduced to an integral in the variable x, as eq 19 shows, which has to be evaluated numerically.

It is worth noting that in the case of mutual diffusion between two clusters, when their approaching distance r becomes smaller than a certain value, the integral given by eq 19 can become so large that their mutual diffusion coefficient, $D_{i,j}(r)$ given by eq 14, drops to zero. Physically, this indicates that during their approach the mutual hindrance induced by the particles belonging to one cluster to the particles belonging to the other becomes so large that their further approach becomes impossible. Thus, the distance where $D_{i,j}(r) \rightarrow 0$ is defined as the minimum approaching distance, r'. Figures 2a and 2b show the values of the normalized minimum approaching distance between two clusters with masses i and j, $r'/(R_{s,i} + R_{s,j})$, as a function of i and j, for DLCA and RLCA clusters, respectively. Note that since both i and j are independent variables, the results are plotted in the form of level curves. As expected, the r' value approaches zero when the difference in masses of the two clusters is substantially large, and it increases progressively as the masses of both clusters increase. Because of the lower particle density for a DLCA cluster compared to a RLCA cluster with the same mass, the values of the minimum approaching distance in Figure 2a are smaller than those in Figure 2b.

2.2.4. Boundary Conditions. To solve eq 11, four boundary conditions have to be specified. The first one, following Smoluchowski, states that the number concentration of clusters

at infinite distance from the reference cluster is equal to the bulk concentration, N_j^0

$$N_j(r) \rightarrow N_j^0 \quad \text{for} \quad r \rightarrow \infty \tag{23}$$

The second and third boundary conditions are obtained by considering the continuity of the concentrations and the fluxes at the boundary between the inner and the outer regions

$$N_j(r)_{r\rightarrow(R_{s,i}+R_{s,j})^-} = N_j(r)_{r\rightarrow(R_{s,i}+R_{s,j})^+}, \tag{24}$$

$$\frac{dN_j(r)}{dr}_{r\rightarrow(R_{s,i}+R_{s,j})^-} = \frac{dN_j(r)}{dr}_{r\rightarrow(R_{s,i}+R_{s,j})^+} \tag{25}$$

where the superscripts + and − refer to the limits taken from the right- and the left-hand side, respectively.

The fourth boundary condition is based on the regularity of the concentration profile of clusters within the reference cluster, i.e.,

$$\frac{dN_j(r)}{dr}_{r=0} = 0 \tag{26}$$

However, as discussed above, there exists a minimum approaching distance, $r' > 0$, where the mutual diffusion coefficient in the inner region drops to zero. Thus, in the numerical solution of eq 11, it is more suitable to use the following boundary condition to substitute for eq 26

$$\frac{dN_j(r)}{dr}_{r=r'} = 0 \tag{27}$$

2.2.5. The Aggregation Kernel, $K_{i,j}$. The overall aggregation rate (or aggregation kernel) between the clusters with mass j and the reference cluster with mass i, $K_{i,j}$, is defined, following Smoluchowski, as the total diffusive flux of the clusters with mass j entering into the inner region of the reference cluster

$$K_{i,j} = 4\pi \frac{D_{i,j}{}^0 (R_{s,i} + R_{s,j})^2}{N_j^0} \frac{dN_j(r)}{dr}_{r=R_{s,i}+R_{s,j}} = 4\pi D_{i,j}{}^0 B \tag{28}$$

where

$$B = \frac{(R_{s,i} + R_{s,j})^2}{N_j^0} \frac{dN_j(r)}{dr}_{r=R_{s,i}+R_{s,j}} \tag{29}$$

Thus, once the gradient term, B, is obtained from solving eq 11 with the boundary conditions, eqs 23, 24, 25, and 26 (or 27), the kernel value $K_{i,j}$ can be readily computed from eq 28.

Some algebraic manipulations may be useful for solving eq 11. The cluster concentration profile in the outer region can be obtained by solving analytically the first equation in eq 11 with the boundary condition eq 23 as follows

$$\frac{N_j(r)}{N_j^0} = 1 - \frac{B}{r} \tag{30}$$

It can be easily shown that from eq 30 the following equation holds true in the outer region

$$N_j(r) + r\frac{dN_j(r)}{dr} = N_j^0 \quad \text{for} \quad r > R_{s,i} + R_{s,j} \tag{31}$$

From this, one can obtain a new boundary condition by combining eqs 24 and 25

$$\left[N_j(r) + r\frac{dN_j(r)}{dr}\right]_{r\rightarrow(R_{s,i}+R_{s,j})^-} = N_j^0 \tag{32}$$

Thus, the second equation in eq 11 with the new boundary conditions, eqs 32 and 27, determines the cluster concentration profile in the inner region. The B constant is then determined through eq 29, where $(dN_j(r)/dr)_{r=R_{s,i}+R_{s,j}}$ is calculated from the numerical solution of eq 11. A numerical solver for boundary value problems based on the orthogonal collocations method, included in the software package Matlab (The MathWorks), has been used. In the following, we will compare the results of the model developed in this section with those obtained using the classical semiempirical kernels, i.e., eq 2 for DLCA and eq 4 for RLCA processes, respectively.

3. Results and Discussion

3.1. Particle−Cluster Aggregation. Let us first consider the case of particle−cluster aggregation. In this case, the model equation, eq 11, is much easier to solve with respect to the case of cluster−cluster aggregation, because the computation of $D_{i,j}(r)$ and $k_{i,j}^*(r)$ (with $j = 1$) in eq 11 does not require any numerical integration, as can be seen from eqs 12 and 13. In addition, such an extreme case is also relevant in real aggregation processes.

3.1.1. Concentration Profiles of the Diffusing Particles. Figure 3 shows the concentration profiles of particles diffusing toward a reference cluster along their approaching distance under DLCA (solid curve) and RLCA (broken curve) conditions, in the case of cluster mass $i = 1000$. The effectiveness factor of collision area, α in eq 13, is set equal to 0.3, and $W = 1$ and 10^3 for DLCA and RLCA, respectively. In the figure, both the particle concentration and the approaching distance are given in dimensionless form, $N_1(r)/N_1{}^0$ and $r/(R_{s,i} + R_P)$, respectively. Then, $r/(R_{s,i} + R_P) > 1$ represents the outer region, while $r/(R_{s,i} + R_P) < 1$ the inner one. It can be seen that because of the introduction of cluster interpenetration, unlike the original Smoluchowski approach, the particle concentration at the collision surface, i.e., $r/(R_{s,i} + R_p) = 1$, does not equal zero under neither DLCA nor RLCA conditions. However, under DLCA conditions, due to the high reactivity of the particles, the concentration of the diffusing particles drops sharply near the collision surface and approaches zero at some location inside

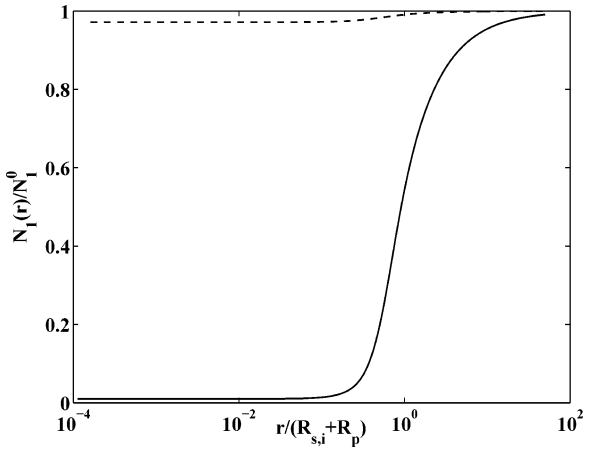

Figure 3. Dimensionless concentration profile $N_1(r)/N_1{}^0$ of the diffusing particles toward a reference cluster with mass $i = 1000$ under DLCA (solid curve) and RLCA (broken curve) conditions, computed through eq 11: $\alpha = 0.3$; DLCA, $W = 1$; RLCA, $W = 10^3$.

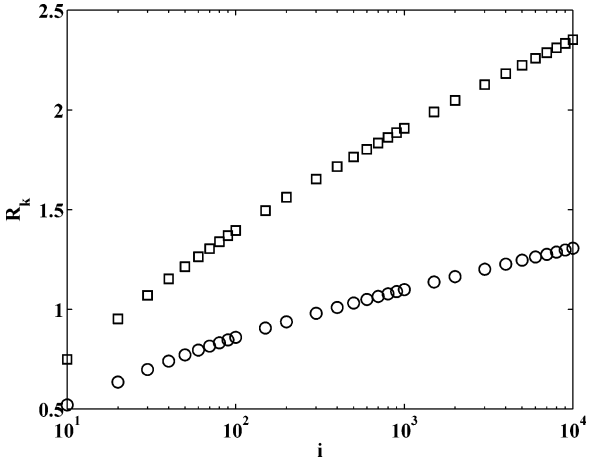

Figure 4. Ratio, R_K, between the values of the particle−cluster DLCA kernel, $K_{i,1}$, computed by eqs 28 and 2, as a function of the cluster mass i, at two different W values: (○) $W = 1$; (□) $W = 2$.

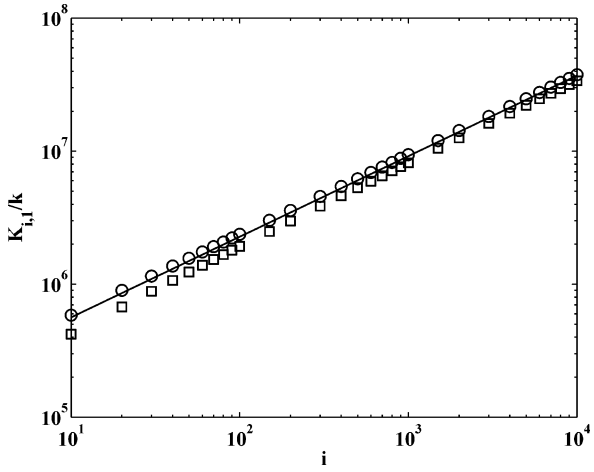

Figure 5. Values of the particle−cluster DLCA kernel, $K_{i,1}$, divided by the Boltzmann constant k, predicted by the present model (eq 28), at two different W values: (○) $W = 1$; (□) $W = 2$. The solid curve is the fitting of the model predictions using the scaling, eq 33, with $1/D_f = 0.606$ and $\alpha = 0.3$.

the cluster. Instead, under RLCA conditions, since the reactivity of the particles is very low in the case of $W = 10^3$, the particles can penetrate much more into the cluster. Although the concentration of the diffusing particles decreases, in fact, while moving toward the center of the cluster due to their reaction with the particles belonging to the cluster, it remains substantially high within the entire cluster.

The slope of the concentration profile of the diffusing particles at $r/(R_{s,i} + R_p) = 1$ gives the estimate of the B value, based on eq 29, and consequently, of the aggregation kernel, $K_{i,1}$, from eq 28. As can be seen from Figure 3, the value of this slope under DLCA conditions is much larger than that under RLCA conditions, and as a result, the $K_{i,1}$ value is larger for DLCA than that for RLCA.

3.1.2. $K_{i,1}$ under DLCA Conditions. The value of the aggregation kernel under DLCA conditions in the case of particle−cluster aggregations, $K_{i,1}$, computed by the model developed in this work, is shown in Figure 4, in terms of the ratio, R_K, to the corresponding value given by the classical DLCA kernel expression, eq 2, as a function of the cluster mass i. In all computations, the effectiveness factor of collision area, α in eq 13, is set equal to 0.3, but two values for the stability ratio, $W = 1$ and 2, have been used. It can be seen that in the case of $W = 1$, the ratio R_K is in the range between 0.5 and 1.3 and increases progressively as the cluster mass increases. This means that, although the two approaches are based on a different derivation, the difference in the predicted $K_{i,1}$ values is not substantial. The slight overestimation of the $K_{i,1}$ values by eq 2, i.e., smaller R_K values, in the region of small cluster masses, may result from the assumption that the radius of a cluster with any mass follows the fractal scaling, which leads to slight overestimation of the radius for small clusters.[29]

It is worth noting that in Figure 4, when the W value changes from 1 to 2, the R_K value at any given i is almost doubled. To identify the source of this variation, let us consider the absolute values of the aggregation kernel, $K_{i,1}$, computed by eq 28 and shown in Figure 5. It is seen that when the W value changes from 1 to 2 the maximum variation in the $K_{i,1}$ value predicted by eq 28 is only about 35% (and it occurs with the smaller cluster mass $i = 10$), which cannot explain the difference in the R_K values in Figure 4. This indicates that the significant difference in the R_K values at two different W values in Figure 4 results from the $K_{i,1}$ value computed by eq 2, which is more sensitive to the variation in W. In addition, from Figure 5, the difference in the $K_{i,1}$ value at two W values increases as the cluster mass i decreases. This arises because small clusters are more compact and tend to behave more like spherical particles, which are more sensitive to the change in W.

From eq 13, we see that decreasing the effectiveness factor of the collision area, α, has the same effect as increasing the W value. Thus, the results in Figure 5 can also be used to conclude that small variations in the α value do not change significantly the $K_{i,1}$ value for clusters with substantially large mass i. This arises because for large clusters the number of particles available for the collision is so large that a small decrease in the effectiveness factor of the collision area leads to an insignificant variation in the penetration depth of the diffusing particle into the cluster and thus in the aggregation kernel.

In the case of particle−cluster aggregation, it can be easily derived from the classical kernel expression, eq 2, that the DLCA kernel scales with the cluster mass i according to the following law

$$K_{i,1} \sim i^{1/D_f}. \tag{33}$$

Since i^{1/D_f} represents the characteristic size of the cluster with mass i ($i^{1/D_f} \sim R_{s,i}$), eq 33 states that the $K_{i,1}$ value is linearly proportional to the cluster size. Considering that the fractal dimension D_f of the DLCA clusters is 1.85, the exponent, $1/D_f$ in eq 33, is 0.54. However, when the $K_{i,1}$ values in Figure 5 are fitted with the above scaling, as given by the solid curve in Figure 5, the obtained value for the exponent is 0.606, significantly larger than 0.54, indicating that $K_{i,1}$ increases with i faster than the cluster size. This result reveals that according to the model developed in this work the reactivity of a fractal cluster cannot be considered to be linearly proportional to its size, as often assumed. This can be understood from the definition of $K_{i,j}$, eq 28, which in the case of particle−cluster aggregation reduces to

$$K_{i,1} \sim R_{s,i} \frac{d[N_1(r)/N_1^0]}{d[r/(R_{s,i} + R_p)]}^{r=R_{s,i}+R_p} \tag{34}$$

This equation states that if the reactivity of a fractal cluster is linearly proportional to its size, then the dimensionless surface gradient of the particle concentration has to be independent of the size of the cluster. To demonstrate that the latter does not hold true, we have computed the dimensionless concentration

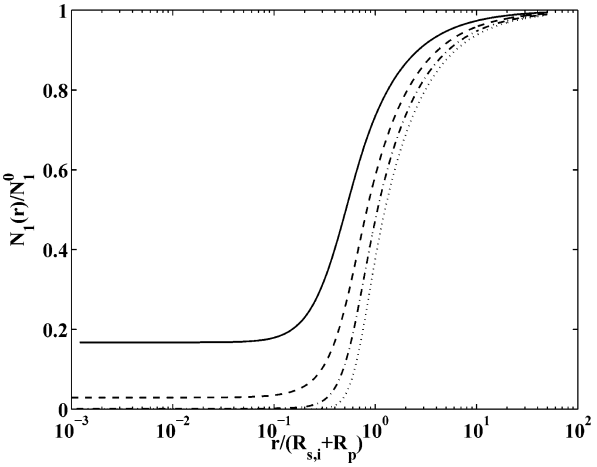

Figure 6. Dimensionless concentration profiles $N_1(r)/N_1^0$ under DLCA conditions of the diffusing particles toward a reference cluster with mass $i = 10$ (solid curve), $i = 100$ (broken curve), $i = 1000$ (dash−dotted curve), and $i = 10\,000$ (dotted curve), computed by eq 11: $\alpha = 0.3$; DLCA, $W = 1$.

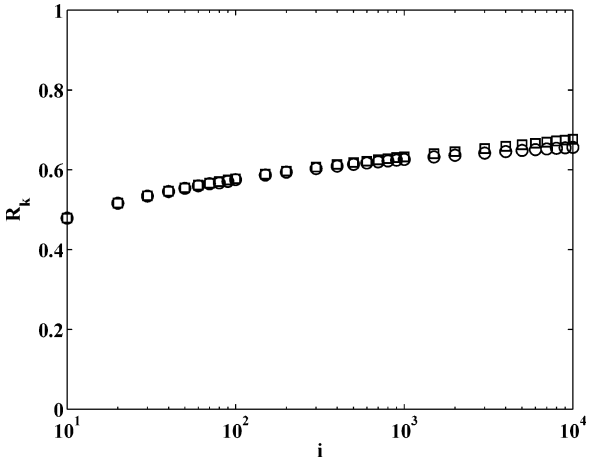

Figure 7. Ratio, R_K, between the values of the particle−cluster RLCA kernel, $K_{i,1}$, computed by eqs 28 and 4, as a function of the cluster mass i, at two different W values: (○) $W = 10^6$; (□) $W = 10^3$; $\alpha = 0.3$; $\lambda = 0.5$; $N_{1,1} = 1$.

profiles of diffusing particles toward a cluster of mass $i = 10$, 100, 1000, and 10 000, respectively, and the results are shown in Figure 6. It is clear that the dimensionless surface gradient (i.e., at $r/(R_{s,i} + R_p) = 1$) of the particle concentration increases as the cluster size increases, thus enhancing the aggregation rate. On physical grounds, this may be related to the relative penetration depth of the diffusing particles into the cluster, which decreases as the cluster mass i increases, leading to the effective collision radius increasing with i faster that its real radius.

3.1.3. $K_{i,1}$ under RLCA Conditions. Typical predictions of the developed model under RLCA conditions are shown in Figure 7, again in the form of R_K, which is now defined as the ratio of the aggregation kernels computed by the present model, eq 28, and by the classical RLCA kernel expression, eq 4. The α value in eq 28 is again set equal to 0.3, and two substantially different values of the Fuchs stability ratio, $W = 10^3$ and 10^6, have been used. Following the previous investigations in the literature,[9,20] in eq 4 we set $\lambda = 0.5$ and $N_{1,1} = 1$. It is found that the results for $W = 10^3$ and 10^6 are practically overlapped, indicating that in the RLCA regime both the developed model and eq 4 predict the same effect of W on the aggregation kernel. In addition, the R_K values increase slightly as the cluster mass i increases but remain confined in a small range, between 0.4 and 0.7, which indicates that the developed model and the RLCA kernel, eq 4 with $\lambda = 0.5$, give very similar predictions of the $K_{i,1}$ values.

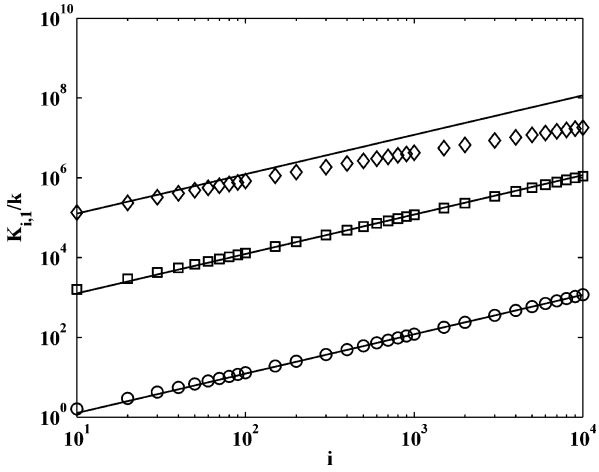

Figure 8. Values of the particle−cluster RLCA kernel, $K_{i,1}$, divided by the Boltzmann constant k, computed by the developed model (eq 28), at three W values: (○) $W = 10^6$; (□) $W = 10^3$; (◇) $W = 10$. The solid curves are the fittings of the model predictions using the scaling, eq 35, with $D_f = 2.05$, $\lambda = 0.5$, and $\alpha = 0.3$.

As mentioned in the Introduction, for RLCA processes with sufficiently small values of the Fuchs stability ratio W, a crossover, i.e., the transition of the aggregation kinetics from RLCA to DLCA, can occur as the clusters grow. The RLCA kernel, eq 4, predicts such a crossover when the product term, $(ij)^\lambda$, becomes substantially larger than W. In particular, the particle−cluster aggregation rate constant under DLCA conditions scales with the cluster mass i as given by eq 33, i.e., with a scaling exponent equal to $1/D_f$, while in the case of RLCA it scales as follows

$$K_{i,1} \sim i^{1/D_f+\lambda} \tag{35}$$

During the transition from RLCA to DLCA kinetics, the scaling exponent predicted by eq 4 reduces from $1/D_f + \lambda$ to $1/D_f$, i.e., from 0.988 to 0.488. To investigate how the model developed in this work predicts the scaling of the kernel with the cluster size and in particular the crossover phenomenon, we have plotted in Figure 8 the $K_{i,1}$ values computed by eq 28 as a function of i, at three different values of $W = 10$, 10^3, and 10^6. The solid lines are the scaling given by eq 35 using $D_f = 2.05$ and $\lambda = 0.5$, i.e., the scaling exponent $1/D_f + \lambda = 0.988$. It is seen that in the case of $W = 10^3$ and 10^6 the $K_{i,1}$ values predicted by the present model follow closely the scaling, at least in the considered range of cluster sizes, while in the case of $W = 10$ only the values corresponding to small clusters follow the scaling in eq 35. As the cluster size increases, the value predicted by eq 28 becomes progressively smaller than that given by the scaling due to the occurrence of the crossover from RLCA to DLCA kinetics. This indicates that, as already seen in Figure 7, the developed model is able to predict crossover from RLCA to DLCA. Note that in the case of $W = 10$ in Figure 8 the predicted $K_{i,1}$ value progressively deviates from the scaling line with exponent $1/D_f + \lambda = 0.988$, and for the largest considered clusters it exhibits a scaling exponent of 0.688 instead of 0.488, indicating that the transition to DLCA is not yet complete.

3.2. Cluster−Cluster Aggregation. *3.2.1. $K_{i,j}$ under DLCA Conditions.* In the case of a diffusing cluster with mass j aggregating with a reference cluster with mass i under DLCA

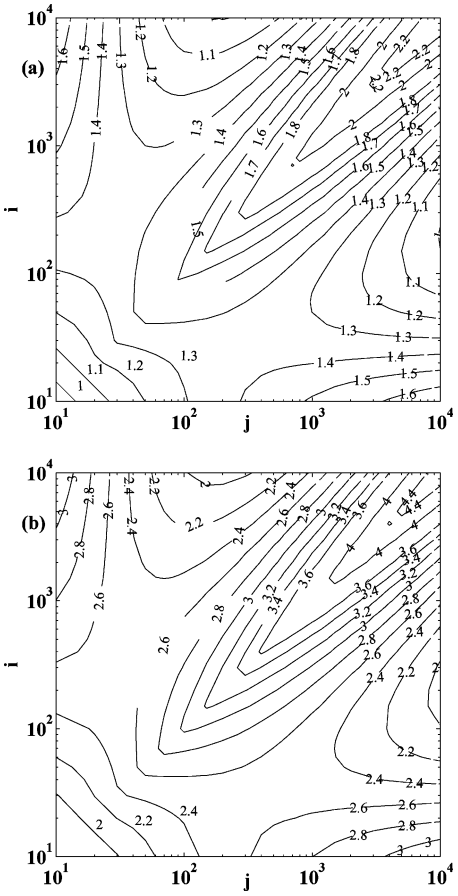

Figure 9. Ratio, R_K, between the values of the cluster−cluster DLCA kernel, $K_{i,j}$, computed by eqs 28 and 2, as a function of the masses of the two clusters, i and j, in the form of level curves: $\alpha = 0.3$; (a) $W = 1$; (b) $W = 2$.

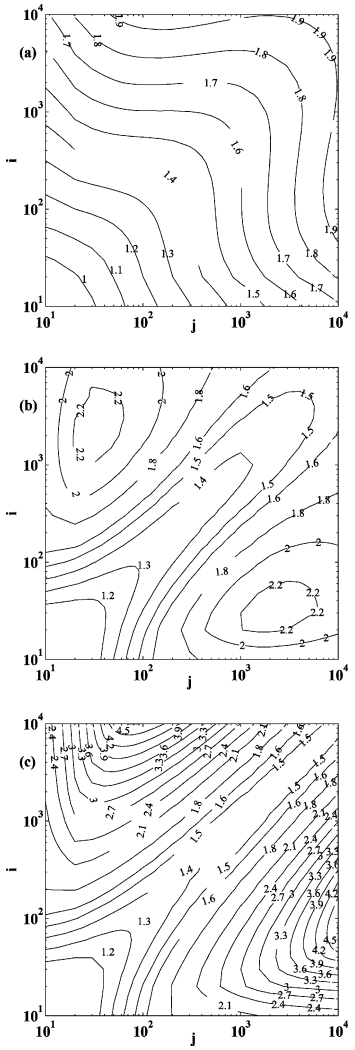

Figure 10. Ratio, R_K, between the values of the cluster−cluster RLCA kernel, $K_{i,j}$, computed by eqs 28 and 4, as a function of the masses of the two clusters, i and j, in the form of level curves: $\alpha = 0.3$; $\lambda = 0.5$; $N_{1,1} = 1$; (a) $W = 10$; (b) $W = 10^3$; (c) $W = 10^6$.

conditions, Figures 9a and 9b show the values of the aggregation kernel, $K_{i,j}$, as a function of the masses of the two clusters, predicted by the developed model, eq 28, corresponding to $W = 1$ and $W = 2$, respectively, and $\alpha = 0.3$. Note that the results are again presented in the form of the ratio, R_K, between the $K_{i,j}$ values computed by eqs 28 and 2. Moreover, since both i and j are independent variables, it is more suitable to plot the R_K values in the form of level curves. The results in Figure 9a indicate that similarly to the case of particle−cluster aggregation, the R_K value increases progressively as the masses of the two clusters, i and j, increase. When one of i and j or both are small, the R_K values are very close to unity, that is, the $K_{i,j}$ values predicted by the developed model are very close to those computed by eq 2, while in the case where both i and j are large, the R_K value can be as large as 2.2.

When the W value changes from 1 to 2, the R_K values in Figure 9b, compared to those in Figure 9a, are almost doubled. It can be easily shown that as in the case of the particle−cluster aggregation the $K_{i,j}$ value predicted by the developed model is less sensitive to the change in W with respect to that computed by eq 2. This arises because in the developed model the reduced reactivity due to the increase in W is partially compensated for by a slightly deeper interpenetration between the clusters, while the $K_{i,j}$ value computed by eq 2 is inversely proportional to W. In addition, the results in Figures 9a and 9b also indicate that the model prediction is insensitive to small changes in the effectiveness factor of collision area, α.

3.2.2. $K_{i,j}$ under RLCA Conditions. The $K_{i,j}$ values under RLCA conditions are shown in Figures 10a, 10b, and 10c, for $W = 10$, 10^3, and 10^6, respectively, again in the form of the ratio, R_K, between the $K_{i,j}$ values computed using eqs 28 and 4. It can be seen that the predictions of the developed model are again very close to those given by the RLCA kernel expression, eq 4. It is worth noting that, contrary to the DLCA case, the largest deviations occur for aggregations between small and large clusters, and they increase as W increases, so that for $W = 10^6$ a maximum R_K value of about 4.5 is obtained. This occurs because when W is substantially large the small cluster may penetrate entirely into the large cluster, leading to more particles available for the reaction.

To better understand the behavior of the predicted RLCA kernel by the developed model, let us consider the special case where the masses of the two aggregating clusters are identical. In this case, the absolute values of the aggregation kernel predicted by the developed model are shown in Figure 11 as a function of the cluster mass for three W values considered above. It is seen that similarly to the cases in Figure 8 as the W value reduces from 10^6 to 10, due to the transition from RLCA to DLCA regime, the flattening of the $K_{i,j}$ curve as a function of the cluster mass occurs for larger values of the cluster mass.

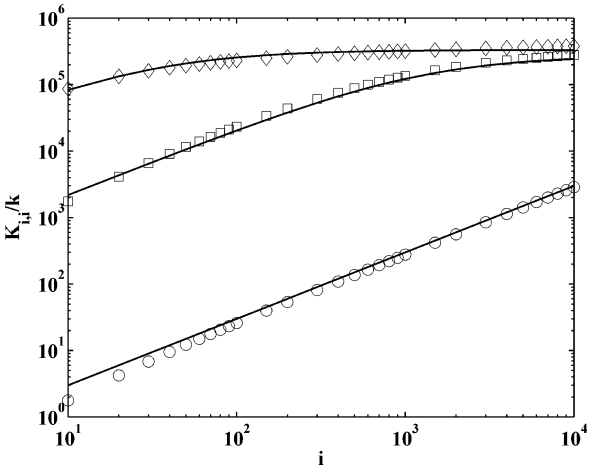

Figure 11. Rate of cluster−cluster aggregation, for clusters of equal mass, divided by the Boltzmann constant k, in RLCA conditions computed through eq 28, for three values of the Fuchs stability ratio W: (○) $W = 10^6$; (□) $W = 10^3$; (◇) $W = 10$. The curves are obtained by fitting the data points according to eq 36, with $D_f = 2.05$ and $\lambda = 0.5$.

In the case of aggregation between equal size clusters, the RLCA kernel expression, eq 4, reduces to the following form

$$K_{i,j} \sim \frac{N_{1,1}(ij)^{\lambda}}{1 + \frac{(N_{1,1}(ij)^{\lambda} - 1)}{W}} \quad \text{with} \quad i = j \tag{36}$$

The predictions of the developed model in Figure 11 have been fitted with this equation, and the obtained results are shown in the figure by the solid curves. It can be seen that the scaling of the model predictions with the cluster mass is well captured by eq 36 in all three cases. The estimated parameter values are $\lambda = 0.5$ for all W values, while different values have been obtained for parameter $N_{1,1}$: $N_{1,1} = 0.3$ for $W = 10$, $N_{1,1} = 0.8$ for $W = 10^3$, and $N_{1,1} = 1$ for $W = 10^6$; i.e., the $N_{1,1}$ value tends to increase as W increases. Since in the original derivation[24] of eq 4 $N_{1,1}$ was considered to be the mean number of collisions per event between a pair of particles, one should indeed expect its value to increase as W increases. However, to keep its physical meaning, $N_{1,1}$ should have a minimum value of one per aggregation event. Thus, all values of $N_{1,1}$ smaller than 1 obtained from fitting our model indicate that $N_{1,1}$ does not have the same physical meaning as that in its original derivation.

From the above results, we can conclude that the RLCA kernel expression, eq 4 with $\lambda = 0.5$ and $N_{1,1}$, provides a reasonable approximation of the results of the model developed in this work, and therefore, being in closed form, it can be most conveniently used in population balance simulations. Moreover, the present model gives a physically sound interpretation of the product aggregation kernel. In particular, it predicts that the relative interpenetration depth between large clusters is smaller than that between small clusters, and therefore, as the cluster mass increases, the effective cluster size for aggregation increases faster than the real size, as implied by the product term. It is worth noting that the same model under DLCA conditions predicts that this feature is not present, and in fact small−large aggregations prevail over large−large ones.

3.3. Structure of the Cluster Formed after Aggregation. To estimate the structure of the new cluster formed after aggregation of two clusters, we need first to compute the radius of gyration of the new cluster. The radius of gyration of an object is defined as the square root of the ratio between the moment of inertia of the object, computed with respect to its center of mass, and its mass. Thus, when two clusters with masses i and j interpenetrate and aggregate at a distance r_{i+j} between their centers of mass, the radius of gyration $R_{g,i+j}$ of the newly formed cluster is given by

$$R_{g,i+j}^{\ 2} = \frac{ij}{(i+j)^2} r_{i+j}^{\ 2} + \frac{i}{i+j} R_{g,i}^{\ 2} + \frac{j}{i+j} R_{g,j}^{\ 2} \tag{37}$$

where $R_{g,i}$ is the radius of gyration of the cluster with mass i. From this, the fractal dimension of the new cluster can be estimated based on the fractal scaling

$$i + j = \left(\frac{R_{g,i+j}}{R_p}\right)^{D_f} \tag{38}$$

Note that there must be a prefactor on the right-hand side of eq 38, whose value is slightly smaller than one for RLCA clusters and slightly larger than one for DLCA clusters.[29] Since our main purpose is to verify the fractal scaling, for simplicity, in the following we set such a prefactor equal to 1.

To use eq 37 to compute the radius of gyration of the new cluster, we need to determine the distance r_{i+j} between the mass centers of the two clusters in the new cluster. However, the solution of the model equations, eq 11, supplies only the concentration profile $N_j(r)$ of the clusters with mass j as a function of the distance r from the center of the reference cluster with mass i. However, if one computes the local aggregation rate of the clusters with mass j as a function of r, which is given by $k^*_{i,j}(r)N_j(r)$, one can find that this quantity exhibits a maximum. A typical example is shown in Figure 12, in the case of the aggregation between two DLCA clusters with $i = 10\,000$ and $j = 5000$, respectively. Such a maximum arises because, as shown in Figure 3, $N_j(r)$ decreases as the distance r decreases, while $k^*_{i,j}(r)$ increases as the distance r decreases, so that their product exhibits a maximum. Since the position of such a maximum corresponds to the distance where the largest amount of clusters aggregates, we will use this as a measure of the distance r_{i+j} between the two clusters i and j in the new cluster after aggregation.

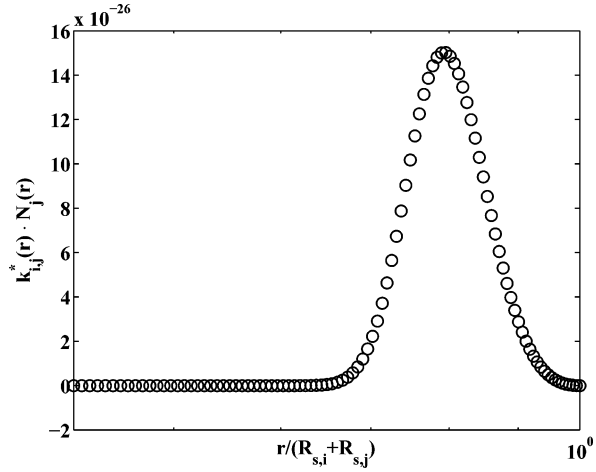

Figure 12. Local rate of consumption of clusters with mass j, $k^*_{i,j}(r)N_j(r)$, in the case of aggregation between clusters with masses $i = 10\,000$ and $j = 5000$, under DLCA conditions with $W = 1$.

It should be mentioned that the choice of the distance at the point where the $k^*_{i,j}(r)N_j(r)$ function reaches a maximum value is reasonable since its peak is quite narrow. In fact, we have

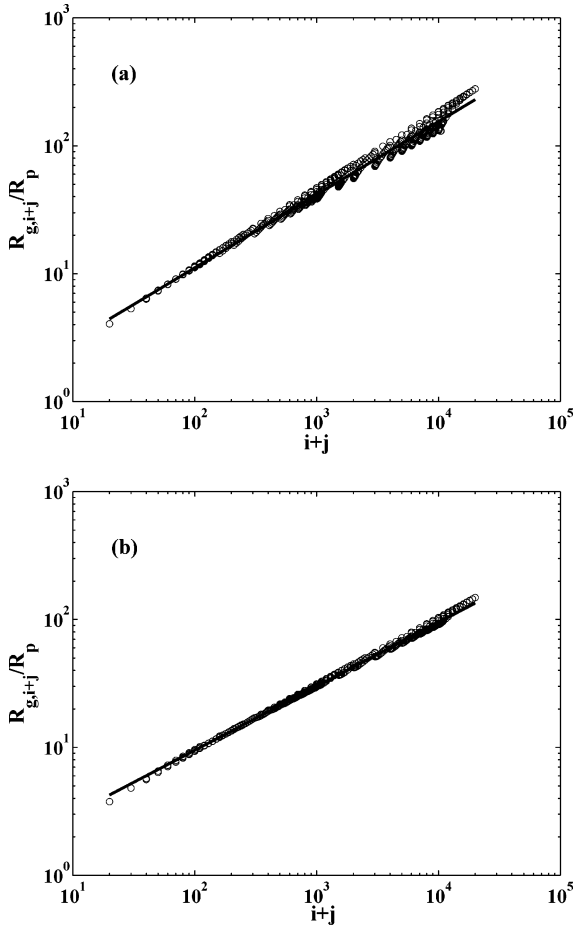

Figure 13. Values of the radius of gyration of the new cluster formed through the aggregation of two clusters with masses i and j, $R_{g,i+j}/R_p$, computed through eq 37, as a function of its mass, $i + j$. (a) DLCA with $W = 1$, and the straight line corresponds to the fractal scaling with $D_f = 1.75$; (b) RLCA with $W = 10^6$, and the curve corresponds to the fractal scaling with $D_f = 2$.

compared the position of the peak with the average value of the aggregation distance r_{av}, defined by the following equation

$$r_{av} = \frac{\int_{r'}^{R_{s,i}+R_{s,j}} 4\pi r^3 k^*_{i,j}(r) N_j(r)\, dr}{\int_{r'}^{R_{s,i}+R_{s,j}} 4\pi r^2 k^*_{i,j}(r) N_j(r)\, dr} \qquad (39)$$

We have found that the difference between the values of fractal dimensions estimated using r_{av} and those obtained using the position of the maximum of $k^*_{i,j}(r)N_j(r)$ is smaller than 1%. Therefore, for the sake of simplicity, the position of the maximum of $k^*_{i,j}(r)N_j(r)$ is used as the aggregation distance.

In Figures 13a and 13b, the radii of gyration computed through eq 37 for various combinations of i and j are shown in the log−log plane as a function of the cluster mass $i + j$, for DLCA with $W = 1$ and for RLCA with $W = 10^6$, respectively. It is seen that in both cases the data fall practically on a straight line, thus indicating that the structures of the clusters formed based on the present aggregation model are consistent with the fractal scaling. From the slope of the curves in Figures 13a and 13b, we estimate the following values of the fractal dimension: $D_f = 1.75$ for DLCA and $D_f = 2.0$ for RLCA. These values, though slightly smaller than those of the aggregating clusters, are consistent with the fractal scaling of DLCA and RLCA clusters.

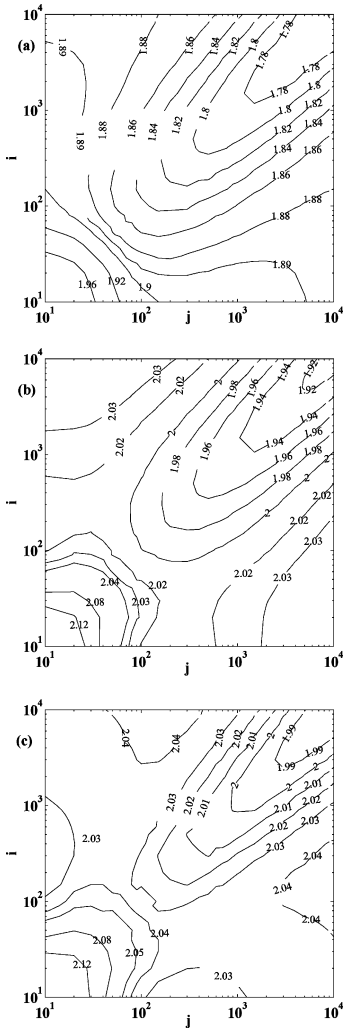

Figure 14. Fractal dimension, D_f, of the new cluster formed through the aggregation of two clusters with masses i and j, as a function of i and j, computed through eq 38, in the form of level curves: (a) DLCA with $W = 1$; (b) RLCA with $W = 10$; (c) RLCA with $W = 10^6$.

However, once the distance r_{i+j} between the two clusters in the new cluster after aggregation is known, the fractal dimension can be computed directly using eq 38, where $R_{g,i+j}$ is given by eq 37. Figures 14a, 14b, and 14c show the fractal dimension obtained in this way as a function of the masses of the two colliding clusters, for DLCA and RLCA with $W = 10$ and RLCA with $W = 10^6$, respectively, again in the form of level curves. It is seen that the values of the fractal dimension in Figures 14a and 14c are in good agreement with the typical values for DLCA and RLCA clusters, respectively. When Figure 14b at $W = 10$ is compared with Figure 14c at $W = 10^6$, one may notice that for a given total mass, $i + j$, the D_f value at $W = 10$ is slightly smaller than that at $W = 10^6$; i.e., the structure of the cluster at $W = 10$ is slightly more open than that at $W = 10^6$. This is consistent with the fact that the extent of interpenetration between clusters becomes less with decreasing the W value, i.e., increasing the reactivity. Moreover, in all the three cases in Figure 14, the D_f value predicted by the model tends to decrease slightly as $i + j$ increases. This indicates that the aggregation between small clusters leads to more compact structures. We also see that for a given total mass, $i + j$, D_f increases as the difference between i and j increases. These results reflect the fact that small clusters penetrate more into large ones.

4. Conclusions

In this work, a model has been developed for describing the aggregation process of two fractal clusters. It is based on the approach originally introduced by Smoluchowski to compute the rate of diffusion-limited aggregation of spherical particles. This approach has been generalized by accounting for both the possibility of interpenetration between clusters due to their open fractal structure and the reactivity (Fuchs stability ratio W) of their particles.

The concentration profile of clusters around a reference cluster is computed by solving the steady-state diffusion-reaction equation, where the reactivity of the clusters is computed based on the reactivity and number of their particles in the interpenetration region. The mutual diffusion between the clusters is described through a radial-dependent mutual diffusion coefficient that accounts for the hindering effect proportional to the concentration of particles in the overlapping region. To evaluate these quantities a radial-dependent particle density distribution computed from suitable Monte Carlo simulations of DLCA and RLCA fractal clusters has been used. The overall aggregation rate or kernel of clusters with the reference cluster is computed based on the overall diffusive flux of clusters toward the reference cluster. The developed model can be applied to predict the aggregation kernel in any (DLCA, RLCA, and transition) regime by simply changing the W value.

It is found that under DLCA conditions the values of the aggregation kernel predicted by the model are close to those given by the most commonly used kernel expression in the literature, i.e., eq 2. However, the obtained scaling exponent of the kernel value with respect to the mass of the cluster is significantly larger than the reciprocal of the fractal dimension, $1/D_f$, indicating that the DLCA kernel is not linearly proportional to the size of the cluster, as often assumed.

In the case of RLCA, the kernel values predicted by our model are in good agreement with those given by the kernel expression proposed by Odriozola et al.,[24] i.e., eq 4, if the exponent λ of the product term in eq 4 is set to equal 0.5. For significantly large clusters, the present model predicts the crossover from RLCA to DLCA kinetics. In addition, by fitting the model predictions with eq 4, it is found that the parameter $N_{1,1}$ in eq 4 increases as the W value increases, but with a value substantially smaller than 6.1, as Odriozola et al. considered.[24]

Since the present aggregation model predicts the center-to-center distance between two clusters in the formed cluster after aggregation, it allows us to compute the radius of gyration of the formed cluster. Then, from the radius of gyration together with the total mass of the cluster, we can estimate the fractal dimension of the formed cluster. It is found that the obtained values of the fractal dimensions under both DLCA and RLCA conditions are in good agreement with those reported in the literature. Moreover, the present model predicts that aggregation between a large cluster and a small cluster leads to a slightly more compact structure with respect to that between two large clusters.

Thus, the developed model for the aggregation rate constant is able to predict, without introducing any empirical parameter, not only the transition from DLCA to RLCA but also the presence in the latter of a term proportional to the product of the masses of the aggregating clusters. It has also been shown that the developed model predicts values of the aggregation rate constants in good quantitative agreement with those computed through the ad hoc kernels previously validated in the literature with experimental data. Moreover, the developed model allows evaluating the structure of the aggregate resulting from the aggregation of two given aggregates, in the form of the fractal geometry. Also in this case the model predictions are in good agreement with the experimental observations.

The developed model provides a tool for evaluating the aggregation rate constant without resorting to the artificial separation between DLCA and RLCA, but simply considering the prevailing operating conditions, and in particular the value of the stability coefficient W.

Acknowledgment. This work was financially supported by the Swiss National Science Foundation (Grant No. 200020-101724). Many useful discussions with Peter Sandkühler and Andrea Vaccaro are gratefully acknowledged.

Notation

A = normalization constant in eq 6, defined in Table 1
B = constant defined by eq 29
D_f = cluster fractal dimension
$D_{i,j}^0$ = mutual diffusion coefficient of clusters in the outer region
$D_{i,j}(r)$ = radial-dependent mutual diffusion coefficient of clusters in the inner region
i = mass or number of particles of the reference cluster
j = mass or number of particles of the diffusing cluster
k_B = Boltzmann constant
$k_{i,j}^*(r)$ = local aggregation rate between particles in the inner region
$K_{i,j}$ = overall aggregation rate or kernel between two clusters with masses i and j
$N_i(t)$ = number concentration of clusters with mass i in the aggregating system at time t
$N_j(r)$ = number concentration of the diffusing clusters at distance r
$N_{1,1}$ = mean number of collisions per event between two particles in eq 4
r = radial distance
r' = minimum approaching distance during mutual diffusion of two clusters
r_{av} = average aggregation distance between two clusters
R_c = cutoff length in $\rho(r)$, defined by eq 6 and in Table 1
$R_{g,i}$ = radius of gyration of a cluster with mass i
R_p = radius of a primary particle
$R_{s,i}$ = characteristic radius of clusters with mass i, defined by eq 7
T = absolute temperature
W = Fuchs stability ratio
z = parameter in $\rho(r)$, defined by eq 6 and in Table 1
α = effectiveness factor of collision area
β = parameter in $\rho(r)$, defined by eq 6 and in Table 1
λ = exponent of the product term in the RLCA kernel, eq 4
$\Gamma(x)$ = Euler gamma function
$\Gamma_{inc}(x)$ = Euler incomplete gamma function
$\rho(r)$ = radial particle density distribution, defined by eq 6

References and Notes

(1) Russel, W. B.; Saville, D. A. S. *Colloidal Dispersion*; Cambridge University Press: London, 1989.
(2) Hunter, R. J. *Introduction to Modern Colloid Science*; Oxford Science Publications: Oxford, U. K., 1994.
(3) Lin, M. Y.; Lindsay, H. M.; Weitz, D. A.; Klein, R.; Ball, R. C.; Meakin, P. *J. Phys.: Condens. Matter* **1990**, *2*, 3093−3113.
(4) Lin, M. Y.; Lindsay, H. M.; Weitz, D. A.; Ball, R. C.; Klein, R.; Meakin, P. *Phys. Rev. A* **1990**, *41*, 2005−2020.
(5) Lin, M. Y.; Lindsay, H. M.; Weitz, D. A.; Ball, R. C.; Klein, R.; Meakin, P. *Nature* **1989**, *339*, 360−362.

(6) Broide, M. L.; Cohen, R. J. *J. Colloid Interface Sci.* **1992**, *153*, 493−508.
(7) Carpineti, M.; Giglio, M. *Phys. Rev. Lett.* **1992**, *68*, 3327−3330.
(8) Carpineti, M.; Giglio, M.; Degiorgio, V. *Nuovo Cimento Soc. Ital. Fis. D* **1994**, *16*, 1243−1246.
(9) Axford, S. D. T. *J. Chem. Soc., Faraday Trans.* **1997**, *93*, 303−311.
(10) Yudin, I. K.; Nikolaenko, G. L.; Gorodetskii, E. E.; Markhashov, E. L.; Agayan, V. A.; Anisimov, M. A.; Sengers, J. V. *Physica A* **1998**, *251*, 235−244.
(11) Meakin, P. *Adv. Colloid Interface Sci.* **1988**, *28*, 249−331.
(12) Meakin, P. *Croat. Chem. Acta* **1992**, *65*, 237−267.
(13) Meakin, P. *Phys. Scr.* **1992**, *46*, 295−331.
(14) Jullien, R. *Croat. Chem. Acta* **1992**, *65*, 215−235.
(15) Whittle, M.; Dickinson, E. *J. Chem. Soc., Faraday Trans.* **1998**, *94*, 2453−2462.
(16) Hütter, M. *J. Colloid Interface Sci.* **2000**, *231*, 337−350.
(17) Odriozola, G.; Tirado-Miranda, M.; Schmitt, A.; Lopez, F. M.; Callejas-Fernandez, J.; Martinez-Garcia, R.; Hidalgo-Alvarez, R. *J. Colloid Interface Sci.* **2001**, *240*, 90−96.
(18) Hanus, L. H.; Hartzler, R. U.; Wagner, N. J. *Langmuir* **2001**, *17*, 3136−3147.
(19) Sandkühler, P.; Sefcik, J.; Lattuada, M.; Wu, H.; Morbidelli, M. *AIChE J.* **2003**, *49*, 1542−1555.
(20) Lattuada, M.; Sandkühler, P.; Wu, H.; Sefcik, J.; Morbidelli, M. *Adv. Colloid Interface Sci.* **2003**, *103*, 33−56.
(21) von Smoluchowski, M. *Z. Phys. Chem.* **1917**, *92*, 129.
(22) Fuchs, N. *Z. Phys.* **1934**, *89*, 736.
(23) Family, F.; Meakin, P.; Vicsek, T. *J. Chem. Phys.* **1985**, *83*, 4144−4150.
(24) Odriozola, G.; Moncho-Jorda, A.; Schmitt, A.; Callejas-Fernandez, J.; Martinez-Garcia, R.; Hidalgo-Alvarez, R. *Europhys. Lett.* **2001**, *53*, 797−803.
(25) Zurita-Gotor, M.; Rosner, D. E. *J. Colloid Interface Sci.* **2002**, *255*, 10−26.
(26) Zurita-Gotor, M.; Rosner, D. E. *J. Colloid Interface Sci.* **2004**, *274*, 502−514.
(27) Lattuada, M.; Wu, H.; Morbidelli, M. *Chem. Eng. Sci.* **2004**, *59*, 4401−4413.
(28) Abramovitz, M.; Stegun, I. A. *Handbook of Mathematical Functions with Formulas, Graphs, and Mathematical Tables*; United States Department of Commerce, National Bureau of Standards: Washington, DC, 1972.
(29) Lattuada, M.; Wu, H.; Morbidelli, M. *J. Colloid Interface Sci.* **2003**, *268*, 106−120.